# Power consumption and form drag of regular and fractal-shaped turbines in a stirred tank

K. Steiros[1], P. J. K. Bruce[1], O. R. H. Buxton[1] and J. C. Vassilicos[1]

[1]*Department of Aeronautics, Imperial College London, SW7 2AZ London, UK*

**Abstract**

Previous wind-tunnel measurements have shown that fractal shaped plates have increased drag compared to square plates of the same area. In this study we measure the power consumption and drag of turbines with fractal and rectangular blades in a stirred tank. Power number decreases from rectangular to fractal impellers by over 10%, increasingly so with fractal iteration number. Our results suggest that this decrease is not caused by the wake interaction of the blades, nor solely by the wake interaction with the walls either.

Pressure measurements on the blades' surface show that fractal blades have lower drag than the rectangular ones, opposite to the wind tunnel experiment results. All tested blades' centre of pressure radius increases with Re, while their drag coefficient decreases, a possible effect of the solid body rotation increase with Re. Spectral analysis of the pressure signal reveals two peaks possibly connected to the blades' roll vortices.

*Keywords:* Rushton Turbine, Pressure Coefficient, Mixing, Power Number, Spectra, Unbaffled

## Introduction

*Stirred tanks*

Tanks stirred by top entering turbines are widely used in the pharmaceutical, chemical and food industries, in applications ranging from blending of homogeneous liquids to solid suspension and gas dispersion to name a few. In all cases the desired property is mixing efficiency, or in other words high mixing quality with low power consumption. Mixing quality depends on the flow field of the vessel, with particular flow field characteristics (e.g. mean field patterns, turbulence intensities) being suitable for different applications. One critical flow aspect for many applications such as homogenizers, colloidal mills and emulsifiers, is the overall turbulence level of the flow[1], making it an indispensable factor in the tank and impeller design.

Apart from the overall turbulence levels, also important is the homogeneity of turbulence in the vessel. High homogeneity is difficult to achieve, given that the injected energy from the impeller quickly decays away from its close vicinity. For instance, the peak dissipation rate for vessels stirred by Rushton turbines is 25-30 times higher in the immediate impeller region compared to the mean dissipation rate[2,3], causing an estimated 60% of the total energy input to be dissipated there[4]. As a result, relatively stagnant regions are created in the rest of the tank, inhibiting complete homogenization and increasing mixing times[5].

A further issue with mixing turbines, especially of the radial type, is the strong localised shear in the impeller discharge region, connected with the tip vortices emanating from the blades[2]. This may create problems in applications where cell membranes and micro-organisms are involved[5] or destroy shear sensitive cells[6].

To address the above issues, extensive research has been centred during the last decades on impeller blade geometry modification[1,5,7,8]. This procedure, mainly done by trial and error, has produced countless impeller types with documented flow fields. The actual improvement however is suggested to be modest at best[5,7]. This underlines the importance of introducing new designs which can contribute to promising results in terms of mixing efficiency. Candidates for this could be the so called fractal/ multiscale objects which have recently been the subject of research in fluid dynamics.

*Fractal generated turbulence*

Fractal/ multiscale objects have been the subject of turbulence research, both experimentally[9–17] and numerically[18,19], over the past decade due to the wealth of phenomena associated with them: Fractal grid turbulence generators[9,10] have been shown to create a longer turbulence production region, and higher turbulence intensities over a wider spatial extent in the decay region, compared to conventional grids. Fractal plates[11,12,17] produce wakes with weaker vortex shedding, higher turbulence intensities and higher local Reynolds numbers, compared to square plates of the same area.

These properties are potentially of interest for many applications, and for this reason fractal geometries applied to grids, trailing edges, and plate perimeters have been investigated for their potential for heat exchange enhancement[14], spoiler aeroacoustic improvement[15,16], static mixing improvement[13,18] and flame control[20] to name a few. Considering the discussion in the previous section it would be interesting to investigate whether the properties described above could be of benefit in stirred tanks, by implementing fractal geometry to the impellers.

One way to do so, is modification of the mixers' blades shape according to the fractal shaped plates introduced by Nedić et al.[11]. This could lead to flows with increased turbulence levels and higher Reynolds numbers, while the plates' weak vortex shedding could contribute to a lower shear near the impeller region.

However, as was demonstrated in wind tunnel experiments[11], fractal plates exhibit higher drag coefficients than square plates of the same area. The experiments showed that this increase is not strongly dependent on *Re*, at least for the tested range, but depends on the fractal iteration number of the plates, as well as on the fractal dimension, with a maximum increase in $C_D$ of the order of 7% (for a definition of the fractal iteration number and fractal dimension see Nedić et al.[11], and later in the text). In the case of an impeller rotating in a tank, an increase in drag of the blades could mean increased power consumption, affecting the overall mixing efficiency. It is therefore important to monitor the power consumption of such impellers, if they are to be implemented.

*Torque and pressure measurements in stirred tanks*

Power consumption in stirred tanks has been commonly calculated by direct measurement of the shaft torque (e.g. through an in line torque transducer). This method has been widely used in the literature[21,22], as it is straightforward and accurate. However, shaft torque does not give any insight regarding the distribution of pressure forces on the blades -which has been estimated to account for around 98% of the total torque in fully turbulent conditions[23]- and the centre of pressure position. Such information is important for design purposes since it is connected to the bending moments and stresses on the blades, causing fatigue and mechanical instability of the agitator[21]. Secondly, pressures at the blade surface are of interest in the case of gas-sparged tanks, since low pressure regions in the rear side of the blades are linked with gas entrainment and cavity formation[21].

Direct pressure measurements on the surface of the blades are therefore necessary, despite this not being a simple task given the rotation of the impeller. Literature on the subject is very limited: Mochizuki and Takashima[24] investigated the effect of the impeller blade curvature on the blade pressure distribution, by using an inverted U-tube manometer mounted on the rotating impeller shaft of curved blade turbines. Tay and Tatterson[23] used a rotating U-tube manometer on a pitched blade turbine to calculate the skin friction contribution on the impeller power consumption, estimating it around 2%. Lane et al.[21] measured the pressure distribution of a Rushton turbine's blades, using a continuous water line from the blades to a stationary pressure cell, in order to compare with CFD, and assess its predictive capabilities. The results showed a reasonable agreement. Mochizuki et al.[25] measured the pressure distribution on the blades of a Rushton turbine in an aerated vessel, using a small pressure sensor mounted on the blades, to investigate the effect of aeration in the blade pressure distribution, showing that the form drag considerably decreases in the case of aeration.

In most of the above works the error (shaft torque calculated via a torquemeter compared to the torque from blade pressure integration) was quite high (up to 10% error for Lane et al.[21] and Mochizuki et al.[25] and up to 30% for Mochizuki and Takashima[24]), while the measurements were not time-resolved. Furthermore, all the above-mentioned works regarding blade pressure distribution, consider baffled tanks only.

Wall baffles are generally installed in transitional and turbulent regimes, since they significantly increase the mixing quality, by breaking the solid body rotation of the flow created by the impeller rotation[26]. However, unbaffled tanks enjoy a growing interest, because the presence of baffles is unwanted in some applications such as crystalizers, or in the pharmaceutical industry where vessel cleaning is of primary significance[6,27]. Nevertheless, despite the

industrial importance of these vessels, experimental data on their performance are still sparse, and properties such as energy injection[27] or mixing times[28] have only recently been investigated.

*Aims of this article*

In this article, we propose a method for measuring the pressure distribution of mixing impellers, using a small pressure sensor and a slip ring, to acquire time-resolved and accurate measurements (i.e. torque calculated from pressure integration matching within a few percent the measured shaft torque). This method is then used to measure the pressure coefficients ($C_p$) on the blades of a radial turbine in an unbaffled tank for the first time, since all similar measurements in the past have been confined to baffled tanks. The turbine is equipped with regular and fractal blades, in order to investigate the differences in their power consumptions, drag coefficients and centres of pressures.

To sum up, the primary aims of this article are as follows:

1. Design of a novel method for measuring time-resolved pressure distributions on the blade surface of mixing turbines.
2. Present for the first time the pressure distribution on the blades of radial turbines in unbaffled stirred tanks.
3. Compare the power consumptions, drag coefficients, centres of pressure and spectral characteristics of pressure, on the blades of fractal and regular bladed impellers.

## Experimental details

*Stirred tank configuration*

Experiments were performed in an octagonal shaped, unbaffled, acrylic tank (fig 1). The tank has an inner diameter of V = 0.45 m and a height H equal to its diameter, while the octagonal shape was chosen to minimize optical distortion in future Particle Image Velocimetry (PIV) measurements. An acrylic lid was positioned on the top of the tank, in order to minimize the effect of the surface vortex caused by the solid-body rotation of the fluid, which was regular tap water.

The impeller used was a radial four-bladed flat blade turbine, mounted on a stainless steel shaft at the tank's mid-height. Three different versions of the impeller were tested (fig 2), by switching acrylic blades on the impeller hub: one with rectangular blades commonly used[26,29], and two with fractal blades, of a design based on the square fractal plates of Nedić et al.[11], which had a fractal dimension of $D_f = 1.5$. The two fractal impellers had one and two fractal iterations respectively (fractal1 and fractal2 henceforth), to investigate the effect of the iteration number in power consumption. All blades had the same area A = 4230 mm$^2$ and same thickness $t$ = 4 mm. While for the regular impeller the diameter and blade width are easily defined, for the fractal cases they are position dependent, due to the shape of the fractals, that consist of small segments. We therefore choose for all three impellers their average diameter values (shaft centre to mean tip distance, see fig 2) D = 223 mm $\simeq$ V/2 and average width h = 44.8 mm (see fig 2).

The impellers were driven by a stepper motor (Motion Control Products, UK) in microstepping mode (25,000 steps per rotation), to ensure smooth movement, which was controlled by a function generator (33600A, Agilent, US). Shaft torque was measured by an in-line torque transducer (TM306, Magtrol, Switzerland), while the rotational speed was monitored with an optical encoder (60ppr) embedded in the torque transducer. Losses due to friction (e.g. from bearings) were monitored by measuring the shaft torque in the tank without water and were subtracted from the actual measurements.

*Blade pressure measurements*

A schematic diagram of the experimental apparatus used for the pressure measurements can be seen in fig 2 and in more detail in fig 3. Measurements were conducted for the regular and fractal1 impellers. In both cases, one of the four blades was substituted with a 3D printed blade with grooves, where the pressure probe (pressure catheter SPR-524, Millar, US) was positioned. As can be seen in fig 3 two types of grooves were made, "wide" grooves ($1.3 \times 5.2$ mm) for the catheter tip (where the sensor area is positioned), and narrower ones for the catheter body. All grooves but the one that the catheter tip was positioned were filled with wax, to make them flush. The positions for both blades where the measurements were taken can be seen in fig 4. The pressure catheter after leaving the blade went through the hollow shaft to the main sensor body that was attached on the shaft above the water. The measurement signal

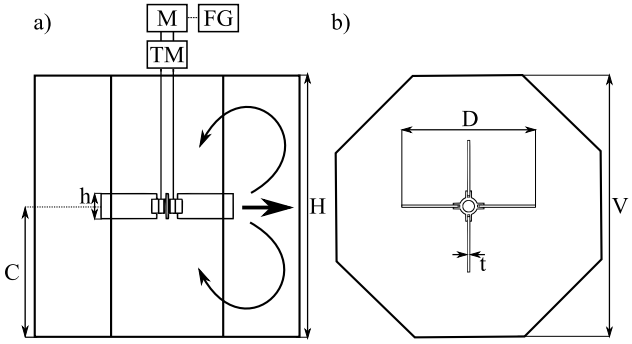


Figure 1: Schematic diagram of the experimental apparatus. TM stands for torque meter, M for stepper motor, and FG for function generator. a) Front view. b) Top view. V=0.45 m, H=V, C=V/2, D=V/2, t=4 mm, h=44.8 mm.

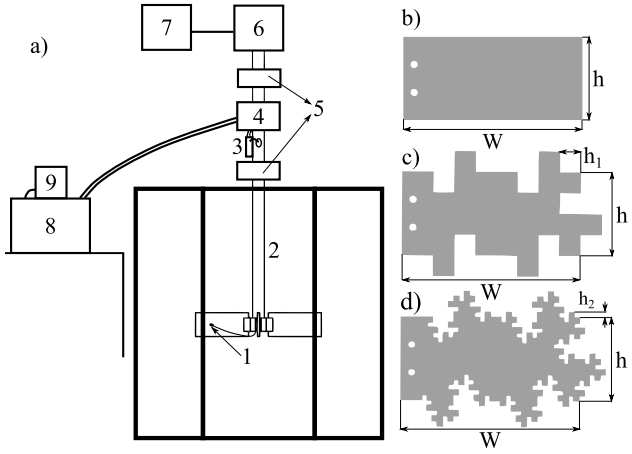


Figure 2: a) Schematic diagram of the experimental apparatus for the pressure measurements. 1) Pressure sensor, 2) hollow shaft, 3) pressure sensor body, 4) slip ring, 5) bearings, 6) motor, 7) function generator, 8) amplifier, 9) DAQ. b) Regular-rectangular blade, c) fractal blade with one iteration (fractal1) and d) fractal blade with two iterations (fractal2). All blades have the same area A=4230 mm$^2$. h=4h$_1$=16h$_2$=44.8 mm, W=95 mm.

and supply sensor voltage were transmitted through a slip ring (SRH Series, Servotecnica, Italy), to an amplifier and finally to the data acquisition system (USB-6211, NI, US). The sampling frequency was set from the DAQ to 1 kHz (the transducer's natural frequency response is 10 kHz), with a low pass filter with a cut-off frequency of 100 Hz, to minimize electrical noise.

In the regular impeller case, 25 locations were measured, over one half of the blade, assuming symmetrical pressure distribution. In the fractal case 39 points were measured spanning all the blade surface. The measurement were conducted one at a time. To measure the pressures on both the front and the rear sides of the blades, measurements were taken for both senses of rotation in the same experimental run (i.e. without moving the probe), by simply reversing the rotation of the shaft. The acquisition time was approximately 60 seconds. We made sure that measurements were reproducible, and then determined the pressure coefficient for each point, i.e.

$$C_p = \frac{P_f - P_r}{1/2\rho U_t^2} \tag{1}$$

where $P_f$ and $P_r$ are the mean pressures in the front and the rear side of the blade respectively, $\rho$ the density of water, and $U_t = \pi ND$ the blade tip velocity ($N$ being the rotational frequency and $D$ the mean diameter as defined in the previous section). Three shaft rotational frequencies were investigated, namely 2, 3 and 4 Hz, corresponding to Reynolds numbers of 100 000, 150 000, and 200 000 respectively ($Re = ND^2/\nu$, $\nu$ being the kinematic viscosity of water). The sensor was calibrated before and after each measurement, by submerging it into different depths of a

graded tube filled with water.

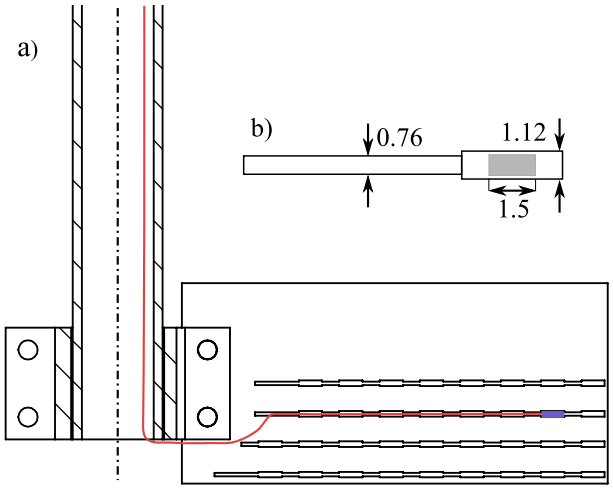


Figure 3: a) Half-section of the impeller equipped with the blade with grooves for the pressure measurements. The catheter (red line) firstly goes through the hollow shaft and then to a groove. The catheter tip, where the sensor lies, is depicted with purple. b) Detail of the pressure catheter tip and sensor area (gray area).

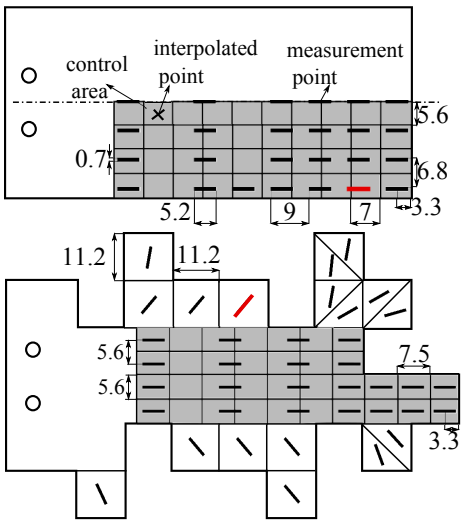


Figure 4: Measurement point positions and control areas for regular and fractal1 blades. In the grey zones the $C_P$ values were interpolated in the middle of the control areas. The red points are the locations where the power spectral densities of the pressure are plotted in figure 10.

*$C_D$, CoP and Torque calculation procedure from $C_P$ values*

The total drag force, $C_D$, torque and centre of pressure (CoP) of each blade was calculated by dividing the blades into control areas (fig 4), and using the following formulae:

$$F = 1/2\rho U_t^2 k \sum_i C_p^i \delta A^i \tag{2}$$

$$C_D = \frac{2F}{\rho U_t^2 A} \tag{3}$$

$$T = 1/2\rho U_t^2 nk \sum_i C_p^i r^i \delta A^i \tag{4}$$

$$CoP = T/nF \tag{5}$$

where $F$ is the drag force of each blade, $T$ is torque, $\delta A^i$ is the control area associated with each point, $n$ is the number of blades, $k$ is a coefficient taking into account whether the control areas span half of the blade or all the blade ($k = 1$ for the fractal1 blade and $k = 2$ for the regular), $A$ is the total blade area, and $r^i$ is the distance of the centre of the control area from the axis of rotation.

For the regular case, one half of the blade was subdivided in 40 control areas (fig 4), while for the fractal1 case the entire blade was subdivided in 51 areas. The pressure coefficients were interpolated in the middle of the control areas where necessary, using a spline interpolation method. In the fractal1 case only the central part of the blade required interpolation (grey area in fig 4), since the measurement points in the other part were already positioned in the centre of the control areas. In the regular blade all points were interpolated.

## Results and discussion

*Steady state power consumption*

Plotted in fig 5 is the variation of the power number $N_p$, with respect to *Re*, for the three types of impellers, along with the correlation relation of Furukawa et al.[22] for rectangular bladed impellers in unbaffled cylindrical tanks. Also plotted are the measured power numbers of a flat blade turbine in a square tank, taken from Xanthopoulos and Stamatoudis[30]. These data correspond to a six-blade turbine, and were therefore scaled down to match the tested four-blade turbines, using the fact that power number is roughly proportional to the blade number in the turbulent regime[31]. The power number is given by the formula[26]:

$$N_p = \frac{T\omega}{\rho N^3 D^5} \tag{6}$$

where $\omega = 2\pi N$ is the angular velocity of the impellers, $\rho$ is the density of water and D is the mean impeller diameter (see section “Stirred tank configuration”).

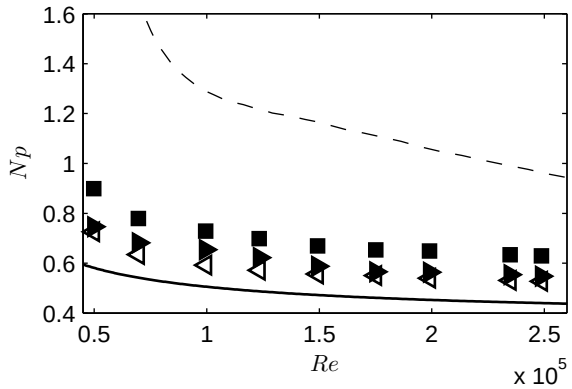


Figure 5: Variation of the power number $N_p$, measured with the torque transducer, with *Re*. (■) Regular blades impeller, (►) fractal1 impeller, (◁) fractal2 impeller. Solid line: correlation relation for rectangular blades impellers in cylindrical tanks[22], dashed line: scaled-down measurements for a flat blade turbine in a square vessel[30].

From fig 5 we observe that the tank’s shape clearly affects the power number values, with the cylindrical vessel power numbers[22], being the smallest of the three vessel shapes. The power numbers of the rectangular impeller in the octagonal vessel are larger by around 35 − 40%, while the data regarding flat blade turbines in square tanks[30] have the largest power numbers, with 40 − 70% difference from the octagonal tank data (note that for the percentage

difference of two values, $y_1$ and $y_2$, throughout the text we use formula $ln(y_2/y_1)100$). The dependence of $N_p$ on the tank shape could be explained from the fact that the corners of tanks act in a similar way to baffles, increasing the power number[26,32]. Moreover, since the octagonal shape lies in between the circle and the square, it is reasonable to expect its power numbers to lie between the two extreme cases as the present results show. For all tank and all blade shapes we observe that the power numbers follow a declining trend, even though *Re* is very large, a phenomenon that has been connected with the absence of baffles[27,30].

Comparing the different tested impellers, we observe that both fractal impellers exhibit a consistent decrease of power number compared to the regular impeller (namely 11 - 12% for the fractal1 impeller and 17 - 20% for the fractal2 impeller). The fractal2 impeller exhibits a decrease in $N_p$ of 3 - 8% compared to fractal1, implying that the power number is affected by the fractal iteration number. It is important to note that the above differences were reproducible.

The decrease of power consumption from the regular to the fractal impellers is seemingly counter-intuitive, given that in wind tunnel experiments[11] fractal square plates of similar design as the current impellers, exhibited *increased* $C_D$ compared to square plates of the same area, as already mentioned in the introduction. To explain this difference, the following possible causes were considered.

A first possibility could be that this reduction is caused by the interaction of the rotating blades' wakes, not possible in the static case. Since the wakes of fractal geometries have been shown in the static case to have higher turbulence intensities[11], this interaction could lead to differences in drag/ torque.

Another possible explanation is that the drag of the fractal impellers is higher than that of the regular impeller, but the centre of pressure is closer to the shaft, therefore leading to a decrease in torque.

Thirdly, the difference could be attributed to the interaction of the turbines' wakes with the tank wall, a factor which may affect the torque differently for each case. This can be understood better if we split the wall torque, $T_w$, in two components

$$T_w = T_\gamma + T_I \tag{7}$$

In the above equation, $T_\gamma$ is caused by the wall friction due to the fluid solid body rotation in the tank. The second term, $T_I$, is caused by the blades' wake interaction with the wall in the following sense: Firstly, the wake impinges on the tank wall due to the radial jet (see fig 1). Subsequently, it spirals up and down and finally it recirculates back to the impeller area. The impingement and spiralling motion of the wake generate friction, which creates the torque $T_I$. Note that the two wall torque components, $T_I$ and $T_\gamma$, can exist independently, e.g. in the case of a "big" tank with very small impeller to tank ratio ($D/V \ll 1$). In that case the impeller wake does not reach the wall ($T_I = 0$) and all measured torque is caused by the solid body rotation, i.e. $T_w = T_\gamma$.

Differences in the wake behaviour of the regular and fractal impellers (e.g. because of weaker/ less coherent vortices due to the fractal shape[11,17]) could therefore lead to a smaller $T_I$ in the case of the fractal impeller. We will now investigate in which way a difference in $T_I$ may influence $T_\gamma$ and the impeller torque, $T_{imp}$, in an unbaffled tank. To do this, we perform the following "thought experiment". We assume two impellers, *A* and *B*, which produce the same $T_{imp}$ in the same flow field, but impeller *A* produces less $T_I$, i.e. $T_{IA} < T_{IB}$. A physical example of this is two impellers which produce the same torque in an infinite medium ($T_w = 0$), or in a "big" tank ($D/V \ll 1$, $T_I = 0$), but we monitor their torque in a "small" unbaffled tank where their $T_I$ is non-negligible and different. Angular momentum balance in the volume of the "small" tank gives

$$T_{imp} = T_I + T_\gamma + \frac{dL}{dt} \tag{8}$$

where $L$, the angular momentum in the tank, quantifies the solid body rotation. The impeller torque is a decreasing function of $L$, since the relative velocity of the blades decreases for increasing solid body rotation. Moreover, $T_I$ is also a decreasing function of $L$, since attributes which make the wake energetic (e.g. the impeller mass flow rate, pressure difference between the blade sides and tip-vortex strength) decrease with increasing solid body rotation. Finally, from its definition $T_\gamma$ is an increasing function of $L$. From the above, equation 8 becomes

$$f(L) = g(L) + w(L) + \frac{dL}{dt} \tag{9}$$

where $f$ and $g$ are decreasing functions, with $h(L) = f(L) - g(L) > 0$, and $w$ is an increasing function. We now write equation 9 for the two impellers, $A$ and $B$. Since we assumed that in the same flow field they would produce the same torque, we have $f_A(L) = f_B(L) = f(L)$. Furthermore, we assumed that impeller $A$ applies less $T_I$ on the wall. Therefore, we have $g_A(L) < g_B(L)$. Finally, since the tank wall is the same for both cases, $w$ is common for both impellers. From the above we have

$$f(L_A) = g_A(L_A) + w(L_A) + \frac{dL_A}{dt} \tag{10a}$$

$$f(L_B) = g_B(L_B) + w(L_B) + \frac{dL_B}{dt} \tag{10b}$$

We now substitute $h_A = f - g_A$ and $h_B = f - g_B$, which are assumed to be decreasing functions of $L$ (this assumption will be investigated in a future work). Note that $h_B(L) < h_A(L)$, since $g_A(L) < g_B(L)$. After the transient effects have subsided, equations 10a and 10b become

$$h_A(L'_A) = w(L'_A) \tag{11a}$$

$$h_B(L'_B) = w(L'_B) \tag{11b}$$

where $L'$ corresponds to the steady state solid body rotation.

- If $L'_A = L'_B$ then from eq 11a and 11b $h_A(L'_A) = h_B(L'_B) = h_B(L'_A)$. This is not possible, since $h_B(L) < h_A(L)$.
- If $L'_A < L'_B$ then from eq 11a and 11b $h_A(L'_A) < h_B(L'_B)$. This is only possible if $L'_A > L'_B$, since $h$ was assumed to be a decreasing function and $h_B(L) < h_A(L)$. This is inconsistent with our first assumption.

Thus, the only possibility is that $L'_A > L'_B$ which means $f(L'_A) < f(L'_B)$, which are the impeller torques, i.e. $T_{impA} < T_{impB}$. The above therefore suggest that an increase in $T_I$ reduces the solid body rotation in the tank, which decreases $T_\gamma$, but the overall $T_{imp}$ increases nevertheless. In other words, it is suggested that even if two impellers produced the same torque under the same conditions, if they were to stir a tank where their $T_I$ differed, they would undergo a transition, and finally the one with the larger $T_I$ would produce a larger steady state torque. This could apply in our case as well, where the fractal objects could produce more drag/ torque compared to regular shaped objects if they are in identical conditions (e.g. wind tunnel experiments, rotation in an infinite medium), but in the case of rotation in a stirred tank the interaction with the wall leads to the fractal objects having less torque.

Finally, the differences between the static and the rotating case could be caused by the effects of the rotation on the flow field of the blades. Firstly, the relative or "free stream" velocity of the rotating blades could be thought as a shear flow with a velocity gradient proportional to the shaft angular velocity, whereas in the wind tunnel experiments the free stream velocity was uniform[11]. Secondly, in the rotating case the centrifugal and Coriolis forces act on the flow, while they are absent in the static case. These forces severely influence the flow field, by producing the radial jet in the rear side of the blades[4], and by altering the wake/ tip-vortices path[33] among others. The above effects could play a significant role in changing the flow separation of the blades, and therefore the overall torque.

The first three possibilities are investigated thereon in the text, while the fourth one requires flow-visualizations and will be part of a future study.

*Wake interaction investigation*

To investigate the first possible cause, the following experiment was carried out: The tank was stirred by a turbine with only two blades, one fractal and one rectangular, placed at 90° to one another, the design of which can be seen in fig 6. Shaft torque measurements were made for both senses of rotation, so that in one case the fractal blade precedes while the rectangular blade is following, and vice versa. If the wake interaction was indeed one of the causes of the torque/ power reduction, then different torques would be measured for each case, since in one case the fractal blade would interact with the wake of the rectangular blade, while in the other case the regular blade would interact with the wake of the fractal blade. In fig 6 the torque measurements over a range of Reynolds numbers are plotted, for both senses of rotation. The two measured torques agree perfectly, showing that the measurement is independent of the rotational sense. This implies that the torque decrease is not caused by the wake interaction of the different blades.

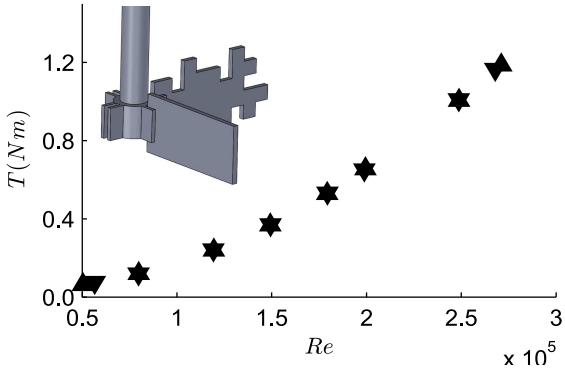


Figure 6: Two-bladed impeller design and measured torque for a range of *Re*. (▼) Clockwise rotation and (▲) counter-clockwise rotation.

*Power consumption at the start of agitation*

As explained in section "Steady state power consumption" the decrease of the power number could be an effect of the tank wall, which could create different flow fields for the regular and fractal impellers. A way to test if indeed the power difference is *only* caused by the wall effect is to monitor the power consumption for the period immediately after the blades begin to rotate in a quiescent fluid ($t = 0$), until the discharged fluid recirculates back to the impeller for the first time ($t = t^*$). During this period the impeller receives fluid with zero angular momentum[34,35] and the behaviour of the turbine could be considered to have similar characteristics to one rotating in an infinite medium[35]. Furthermore, the power number is constant[35], indicating a stationary regime. From the above we can conclude that for $t < t^*$ the wall has no torque-influencing effect on the velocity field of the turbine.

To measure the initial plateau the following experiment was performed: After making sure that the fluid in the tank was at rest, the impeller velocity was immediately increased from zero to a given RPS, corresponding to a given *Re*. An example of the transient power number of the three impellers after the step increase can be seen in fig 7, for the case of $Re = 150,000$. We firstly observe for all three impellers a sharp $N_p$ increase at $t = 0$, when the impeller starts moving, and then the initial plateau for $t < t^* \approx 1.5$ s, where the effects of the wall have not yet affected the impeller torque. At the end of the plateau there is a sharp decrease which corresponds to the discharged impeller fluid reaching the impeller region for the first time. This fluid has non-zero angular momentum, and as a result the blades' relative velocity decreases, along with the impeller power number. Finally, for $t > 11$ s the impellers reach the steady state. The transient power numbers were monitored for a number of *Re* for all three impellers, and the mean of their plateau values, $Np_{inf}$, was calculated for each case.

Plotted in fig 8 are the initial plateau power numbers, $Np_{inf}$, of the impellers with *Re*. We observe that for the two fractal impellers the values are independent of *Re*, while for the regular impeller the power number increases at low *Re*, until it reaches a plateau. This plateau was expected, since the power number of radial turbines in baffled tanks is constant in the fully turbulent regime. Baffles suppress the solid body rotation, and therefore the flow that baffled tanks produce can be thought as having similar properties to the flow at the start of the agitation[34]. By comparing the $Np_{inf}$ of the regular impeller after it has become constant ($Re > 100,000$), with the baffled power number, $Np_b$, of a similar impeller for fully turbulent conditions, taken from Bates el al.[36], we have $Np_{inf} = 4.77$, while $Np_b = 2.67$, i.e. the baffled power number is almost the half of the initial plateau power number. This suggests that baffles do now completely suppress solid body rotation (the tangential velocity of the fluid is not zero). Note that Bates el al.[36] used a six-blade flat blade turbine, and their power number was scaled down to match a four blade turbine, using the fact that the power number is roughly proportional with the blade number[31].

Comparing the initial plateau power number of the regular and the fractal impellers, we observe that the regular impeller exhibits higher values, for all range of tested *Re* i.e. 14-24% higher compared to the fractal1 impeller and 23-31% compared to the fractal2. Note that the percentage differences for the unbaffled case tested before were 11-12% for fractal1 and 17-20% for fractal2. From the above we can deduce that the difference in power number between fractal and regular blades is suggested not to be a result *only* of the tank walls, since it was found also when their effects in the velocity field were absent. Further to that, the percentage difference decreases in the steady state, where

the wall effects are without doubt affecting the flow field. This suggests that the blades' wake interaction with the wall cannot be extremely accentuated in the case of the regular impeller compared to the fractals, otherwise the percentage difference would increase.

Finally, there is a decrease of $Np_{inf}$ from fractal1 to fractal2 impellers by $6-9.5\%$. This difference is slightly larger than for the unbaffled wall case, i.e. $3-8\%$, and it confirms that the power number can be altered by the iteration number.

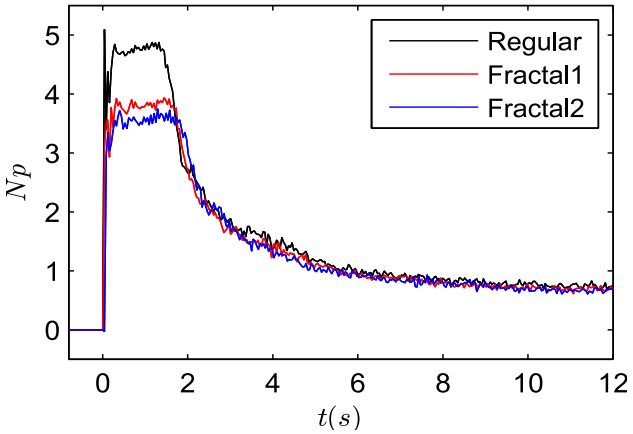


Figure 7: Transient power numbers of the three tested impellers after a step-increase of the shaft velocity from rest ($N = 0$ for $t < 0$) to $N = 3$ RPS ($Re = 150,000$).

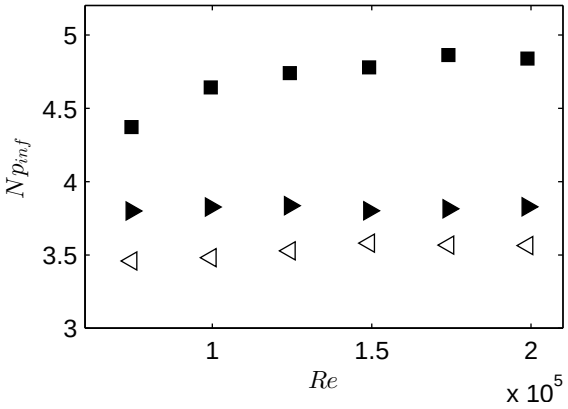


Figure 8: Variation of the initial plateau power number, $Np_{inf}$, with $Re$. (■) Regular blades impeller, (►) fractal1 impeller, (◁) fractal2 impeller.

*$C_p$ distribution*

In figure 9 the values of the pressure coefficient at the measurement points are plotted for the rectangular and fractal1 blades, for three Reynolds numbers. The $C_p$ values of both blades do not change significantly with $Re$, implying self-similarity, something to be expected in fully turbulent conditions[21]. The $C_p$ values on both blades tend to increase with increasing distances from the axis of rotation, due to the increased relative velocities on the blades. This creates higher stagnation pressures on the leading side of the blades[21,25], and possibly increased separation on the rear side of the blades. For the rectangular blade, the highest pressure coefficients are located along the edge of the blade (fig 9, region A). This region has been shown to be connected with roll vortices[21,25,33] created over the rear side of the blades causing low pressures on the rear face. The decrease after this region probably signifies the detachment point of these vortices. In the fractal blade case, the distribution of $C_p$ is asymmetric, with much higher

values in region C, compared to B. This is presumably the result of two non-symmetrical vortices in the rear side of the blade, in regions B and C, with the vortex in region B being the weakest of the two, therefore causing smaller pressure coefficients.

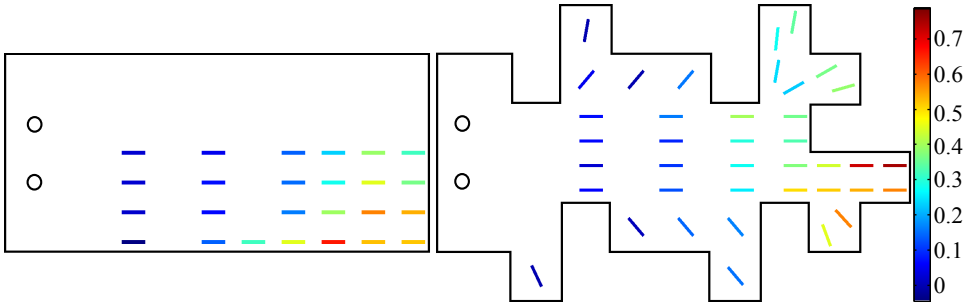


(a) $Re = 100,000$

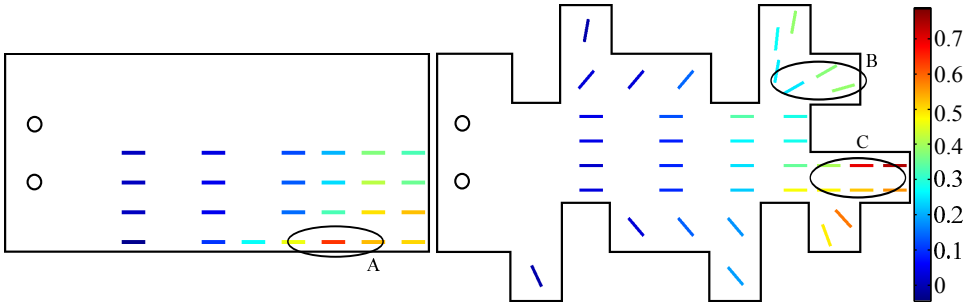


(b) $Re = 150,000$

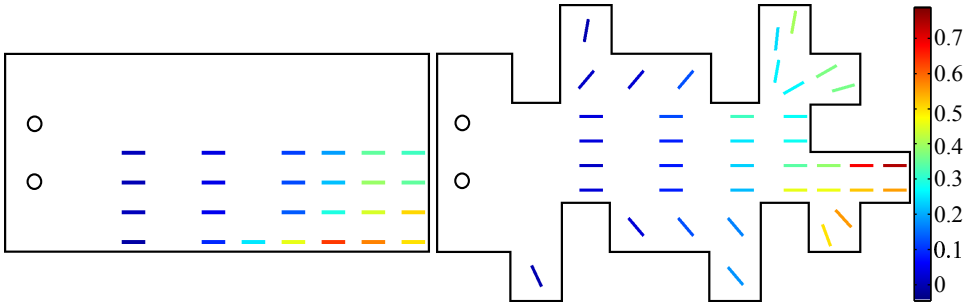


(c) $Re = 200,000$

Figure 9: Measured $C_p$ for regular and fractal1 impellers.

*Drag coefficients and centres of pressure*

The drag coefficients ($C_D$) and centres of pressure (CoP), obtained from the pressure measurements on the basis of formulae 3 and 5, are listed in table 1. For all Reynolds numbers the drag coefficients of the fractal blades have lower values, and their centres of pressure have bigger radii compared to the regular blades. These results are opposite to the conclusions of the stationary experiments[11], where in fact higher $C_D$ was observed for the fractal geometries, and show that the reduced torque observed for both fractal blades cannot be attributed to the change in the centre of pressure, which was one of the listed possible explanations.

For both blades, the CoPs increase slightly but consistently with Reynolds number, with this being possibly due to an increase of the so called "forced vortex"[34]. This is a cylindrically rotating zone around the centre of rotation, where the fluid rotates with almost the same angular velocity as the impeller, therefore causing negligible drag. An expansion of this zone would boost the contribution of the outer side of the blades to the overall blade drag, therefore

| | $C_D$ | | | CoP | | | $R_c$ |
|---|---|---|---|---|---|---|---|
| Re | Reg | F1 | %diff | Reg | F1 | %diff | Reg |
| 100,000 | 0.1716 | 0.1532 | 11.3 | 0.820 | 0.844 | -2.9 | 0.686 |
| 150,000 | 0.1556 | 0.1468 | 5.8 | 0.829 | 0.850 | -2.6 | 0.688 |
| 200,000 | 0.1476 | 0.1416 | 4.2 | 0.832 | 0.853 | -2.5 | 0.689 |

Table 1: Drag coefficients, centres of pressure, and their percentage differences, for the regular and fractal1 impellers. Forced vortex radii ($R_c$) for the regular blade are also shown, derived from the correlation formula of Nagata[34]. The CoPs and $R_c$ are normalized with the radius of the regular blade $D/2$.

| | Regular | | | Fractal1 | | |
|---|---|---|---|---|---|---|
| Re | Pressure | Shaft | %diff | Pressure | Shaft | %diff |
| 100,000 | 0.260 | 0.256 | 1.6 | 0.239 | 0.230 | 3.8 |
| 150,000 | 0.536 | 0.529 | 1.3 | 0.519 | 0.465 | 11.0 |
| 200,000 | 0.907 | 0.911 | -0.4 | 0.892 | 0.792 | 11.9 |

Table 2: Torque in Nm calculated by pressure integration and measuring the shaft torque, and their percentage differences, for the regular and fractal1 impellers.

increasing the CoP. Nagata[34] proposed an empirical formula based on his extensive experimental data to estimate the radius of the forced vortex ($R_c$) in an unbaffled tank, for a range of *Re* spanning from laminar to highly turbulent regimes. Applying the formula in our case for the regular blade impellers (table 1), we observe that the values of $R_c$ have an increasing trend with *Re*, showing that the CoP increase with *Re* could indeed be linked to this phenomenon.

The drag coefficients of both blades drop slightly with *Re*, in agreement with the slight decrease in measured power number (fig 5). This can be explained from the slight increase of the non-dimensional tangential fluid velocity $U_\theta/N$ with *Re* near the impeller, in unbaffled tanks for the turbulent regime, as measured by Yoon et al.[37]. This leads to a decrease of the relative fluid velocity on the impeller, and therefore a decrease in the overall drag.

*Pressure integration versus shaft torque*

By comparing the torque values calculated by pressure integration (eq 4) and shaft torque measurement, we have an estimate of the pressure measurement errors. In table 2 the torque values calculated by pressure integration, the torque values measured with the torque transducer, and the percentage differences between the two are listed.

For the regular case the two ways of measurement show very good agreement, with the pressure measurements only slightly overestimating the expected values, with a maximum overestimation of 1.6%. Naturally, torque calculated by pressure integration does not take into account the skin friction drag contribution, but this is expected to be negligible (i.e. less than 2% of the total torque[23]), not significantly affecting the results.

For the fractal case on the other hand, there is an important overestimation, that increases with *Re*, reaching 11.9%. The origin of this discrepancy may in part be due to a lack of sufficient resolution over the whole blade (e.g. white control areas in fig 4), therefore leading to an inadequate resolution of the complex effects caused by the increased perimeter of the fractal geometry. The probes in those regions measure the pressure in the centre of the control areas, and therefore they don't capture the drop in $C_p$ caused by boundary effects. When integrating, however, the $C_p$ values are assumed uniform in the whole control area, artificially increasing the integral values (i.e. total force, torque and CoP). The sensitivity of these values to the overestimation is discussed in Appendix A, where we show that this may be a significant contributory factor.

*Dynamics of the blade pressure signal*

The final aspect of the blades' pressure distribution that is investigated is its dynamic behaviour. This is important, because it can give us information regarding the structures emanating from the blades. Previous studies that have provided pressure or velocity data in the impeller reference frame measured only statistical quantities[21,23–25,33,38], while time resolved data in stirred tanks in the literature have been provided only for planes stationary relative to the

shaft rotation[4,29,38,39]. This study is therefore the first attempt to date of continuous signal acquisition and spectral analysis in the impeller reference frame.

In fig 10 the power spectral densities of the pressure signal versus normalized frequency $f/N$ ($N$ being the shaft rotational frequency) for the regular and fractal1 blades are plotted. The position of these measurements are the red probe points in fig 4 (points of intense periodicities), while the results for two Reynolds numbers (150,000 and 200,000) are shown for the front and the trailing sides.

A strong periodicity corresponding to a frequency equalling that of the shaft rotation ($f/N$=1) can be seen in all cases, including all other measurement points (not plotted). This peak is often accompanied by harmonics, suggesting a connection with mechanical, or more likely electrical noise due to the slip ring rotation.

To check the validity of this explanation, the following experiment was performed: The pressure transducer was attached to the shaft, which was rotated without mounting the blades. Thus, water was only minimally perturbed, and all variance in the signal was a noise artefact. Plotted in fig 11 are the power spectral densities of the pressure signal versus the normalized frequencies, for shaft rotations equal to the ones used in the actual measurements in fig 10. The peaks at the rotational frequency and its harmonics are evident in both cases, showing that they are the effect of noise. It is important to note that no other peaks are evident in fig 11 showing that all other peaks observed in the PSD plots in fig 10 are not caused by, at least this source of, noise.

In fig 10 energetic peaks can also be observed for frequencies around $f/N = 1.4$, ranging from $f/N = 1.37$ to $f/N = 1.47$ for the regular blade and from $f/N = 1.36$ to $f/N = 1.55$ for the fractal1 blade. These peaks are more energetic for higher *Re*, and are clearly visible only for the measurements taken in the trailing side of the blade. In the front side, only small "bumps" are visible at this frequency (see small bump in the red curve in fig 10a for $f/N = 1.4$), showing that this periodicity is caused by a phenomenon occurring only on the trailing side of the blades. This is a strong indication that these peaks are not an artefact caused by noise. The way in which the experiment was performed, i.e. by consecutively measuring the pressure at the trailing and front sides of the blade at the same measurement point in the same experimental run simply by reversing the sense of rotation, ensures identical experimental conditions on both sides of the blade. Thus, a possible vibration or electrical interference, should be visible in both senses of rotation.

It is interesting to see in which area this periodicity is enhanced, since this information could reveal the location of a possible structure causing it. A qualitative way to do this is to examine the spatial distribution of the peak PSD value around $f/N = 1.4$ for the different measurement points. In fig 12 these distributions, taken from the PSD plots of the measurements on the trailing side of the regular blade, are plotted for *Re* equal to 150,000 and 200,000. In both cases the intensity of the periodicity is increased near the bottom edge of the blade, close to the blade tip. As discussed in section "$C_p$ distribution", this area is close to the detachment region of the roll vortices in the rear side of the blade, and therefore a connection between the two phenomena is conceivable. For the fractal blade on the other hand, no particular trend is evident (fig 13). This could be the effect of the irregular perimeter that breaks the coherent structures[11,17].

Finally, energetic peaks in the PSD plots are also located near $f/N = 0.8$. Such peaks can be found for both senses of rotation, as can be seen for instance in fig 10, while their intensity distributions do not reveal a particular trend.

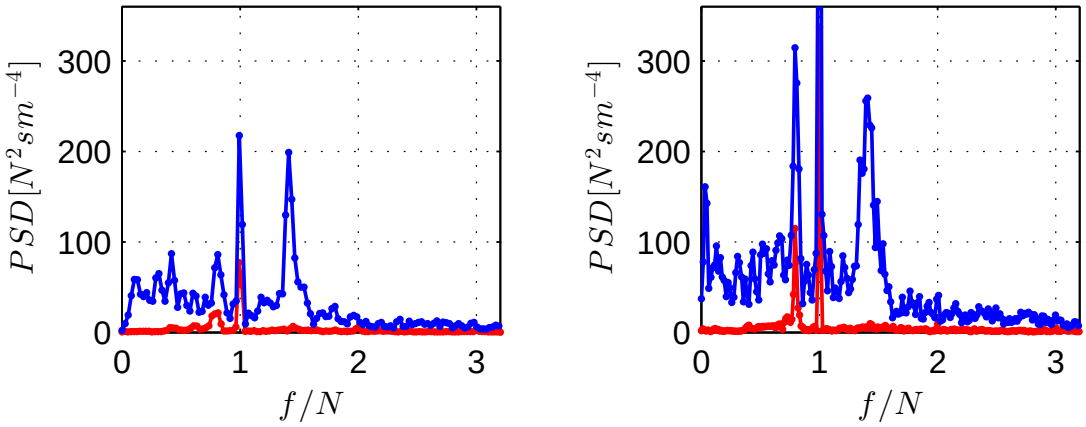


(a) Regular, *Re* =150,000




(b) Regular, *Re* =200,000

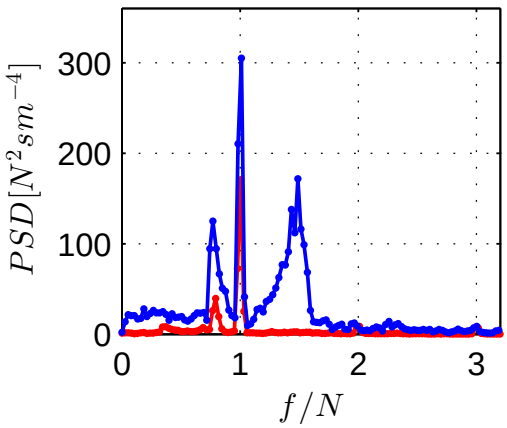


(c) Fractal1, *Re* =150,000

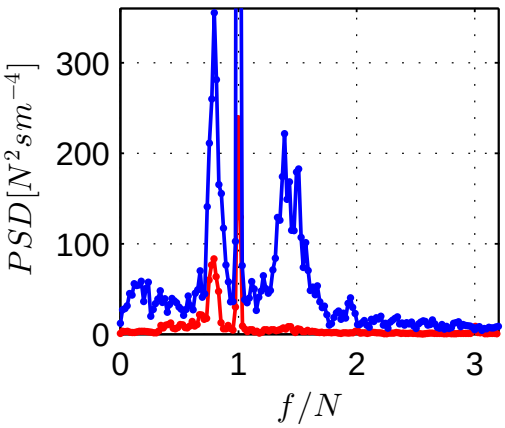


(d) Fractal1, *Re* =200,000

Figure 10: Power spectral density of the pressure signal as a function of frequency $f$ normalised with the shaft rotation frequency $N$, for the regular and fractal1 blades, in the position of the red probes in fig 4. The blue line corresponds to the trailing side of the blade, and the red line to the front side.

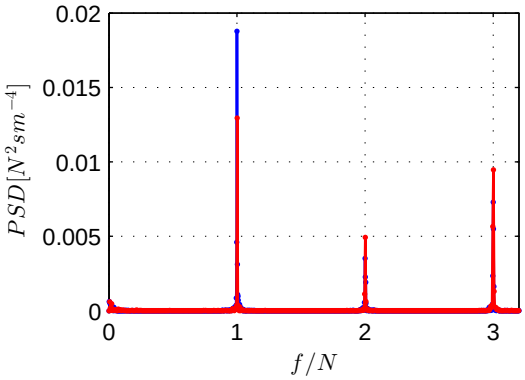


Figure 11: Power spectral densities of the pressure signal $[N^2s/m^4]$ as a function of frequency $f$ normalised with the shaft rotation frequency $N$, for the unbladed shaft case. The red line stands for shaft rotational speed of 3 RPS and the blue line for 4 RPS, corresponding to $Re = 150,000$ and $Re = 200,000$ respectively, for the bladed case.

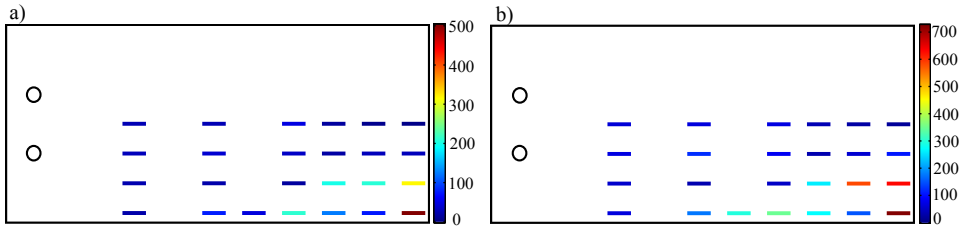


Figure 12: Magnitude of the peak around $1.4f/N$ in the pressure PSD $[N^2s/m^4]$ for the rearward side of the regular blade. a) $Re = 150,000$. b) $Re = 200,000$.

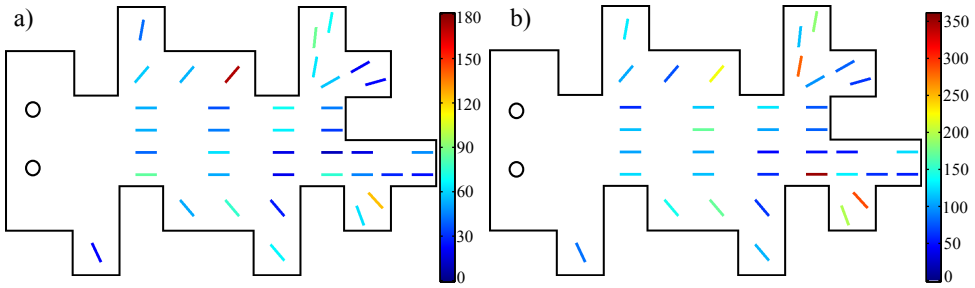


Figure 13: Magnitude of the peak around $1.4f/N$ in the pressure PSD $[N^2s/m^4]$ for the rearward side of the fractal1 blade. a) $Re = 150,000$. b) $Re = 200,000$.

## Conclusions

Three radial turbines, one with regular-rectangular and two with fractal blades following the design of Nedić et al.[11], of one and two fractal iterations respectively (fractal1 and fractal2), were experimentally compared in terms of power consumption in an unbaffled tank at a turbulent regime. The power numbers of two different experimental conditions were monitored. Firstly, the power number of the steady-state regime (SS) and secondly, the power number corresponding to the plateau at the start of the agitation[35] (IP). The regular and fractal1 turbines were also compared regarding their blade pressure distributions for the SS case. All blades had the same area.

Power consumption was monitored from shaft torque and angular velocity measurements, while for the purpose of pressure measurements a novel method for measuring the pressure distribution in rotating turbines was designed, which includes a pressure catheter and a slip ring to transfer the signal. This method provided highly accurate mean values, estimating torque within 1.6% error compared to the expected value, when the measurement spatial resolution was adequate. Furthermore, it enabled for the first time acquisition of time-resolved signals in the impeller reference frame.

Measured power consumption over a range of *Re* for the SS case showed that the fractal1 impeller exhibited a decrease in power number by over 10%, compared to the regular impeller. The fractal2 impeller exhibited a further decrease in power number by over 3% compared to the fractal1 impeller, showing that the iteration number can affect the power input in the tank. In the IP case the fractal1 impeller exhibited a decrease in power number by over 14%, compared to the regular impeller, while the fractal2 impeller exhibited a further decrease in power number by over 6%.

The increased power/ torque of the regular impeller compared to the fractal ones is seemingly counter intuitive, given that in wind tunnel experiments[11] square plates exhibited *smaller* drag coefficients compared to fractal plates of similar design as the blades tested here. Possible causes of this phenomenon were discussed and the validity of three of them was tested: A simple torque experiment showed that the blade wake interaction does not cause the torque reduction. Furthermore, since the power number difference also appeared at the start of the agitation, it is suggested that the tank wall is not the *only* contributory factor to the decrease. Finally, calculation of the blades' drags and centres of pressure (CoP) showed that the regular blades have larger drag coefficients and smaller CoP radii compared

to the fractal1 blades. Thus, it was deduced that the difference in torque between the fractal and regular impellers cannot be attributed to a difference in the position of the centres of pressure of the blades.

The $C_p$ distribution of the blades was found to be almost independent of *Re* implying self-similarity, something to be expected in fully turbulent conditions[21]. The $C_p$ values showed a fairly uniform increase with radius for both blades, with regions of high values being the footprints of the roll vortices in the rear side of the blades. For both cases the CoP radii slightly increased with *Re*, while the drag coefficients decreased slightly, this possibly being attributed to the increase of the "forced vortex" zone radius[34], and fluid non-dimensional tangential velocities[37] with Reynolds number respectively.

Spectral analysis of the pressure signal revealed two dominant peaks at $f \simeq 1.4N$ and $f \simeq 0.8N$ (N being the shaft rotation frequency) for both regular and fractal1 turbines, possibly connected with the roll vortices detachment.

## Acknowledgments

The authors acknowledge support from the EU through the FP7 Marie Curie MULTISOLVE project (Grant Agreement No. 317269). K. Steiros is grateful to Mr F. Giammaria for his help with the instrumentation and to Professor D. S. Mathioulakis for his advice regarding the pressure measurement technique. J. C. Vassilicos acknowledges the support of an ERC Advanced grant (2013-2018).

## Literature Cited

1. Kumaresan T, Joshi JB. Effect of impeller design on the flow pattern and mixing in stirred tanks. *Chem Eng J.* 2006;115:173–193.
2. Sharp KV, Adrian RJ. PIV Study of small-scale flow structure around a Rushton turbine. *AIChE J.* 2001;47:766–778.
3. Baldi S, Yianneskis M. On the quantification of energy dissipation in the impeller stream of a stirred vessel from fluctuating velocity gradient measurements. *Chem Eng Sci.* 2004;59:2659–2671.
4. Wu H, Patterson GK. Laser-Doppler measurements of turbulent-flow parameters in a stirred mixer. *Chem Eng Sci.* 1989;44:2207–2221.
5. Trivellato F. On the efficiency of turbulent mixing in rotating stirrers. *Chem Eng Process.* 2011;50:799–809.
6. Busciglio A, Caputo G, Scargiali F. Free-surface shape in unbaffled stirred vessels: Experimental study via digital image analysis. *Chem Eng Sci.* 2013;104:868–880.
7. Vasconcelos JT, Orvalho SCP, Rodrigues AMAF, Alves SS. Effect of Blade Shape on the Performance of Six-Bladed Disk Turbine Impellers. *Ind Eng Chem Res.* 2000;39:203–213.
8. Georgiev D, Vlaev SD. Fluid Flow Properties of Slotted Flat- and Hollow-blade Impellers. *Chem Biochem Eng Q.* 2008;22:267–272.
9. Hurst D, Vassilicos JC. Scalings and decay of fractal-generated turbulence. *Phys Fluids.* 2007;19:035103.
10. Mazellier N, Vassilicos JC. Turbulence without Richardson-Kolmogorov cascade. *Phys Fluids.* 2010;22:075101.
11. Nedić J, Ganapathisubramani B, Vassilicos JC. Drag and near wake characteristics of flat plates normal to the flow with fractal edge geometries. *Fluid Dyn Res.* 2013;45:061406.
12. Nedić J, Vassilicos JC, Ganapathisubramani B. Axisymmetric turbulent wakes with new nonequilibrium similarity scalings. *Phys Rev Lett.* 2013;111:1–5.
13. Suzuki H, Nagata K, Sakai Y, Ukai R. High-Schmidt-number scalar transfer in regular and fractal grid turbulence. *Phys Scrip.* 2010;T142:014069.
14. Cafiero G, Discetti S, Astarita T. Heat transfer enhancement of impinging jets with fractal-generated turbulence. *Int J Heat Mass Tran.* 2014;75:173–183.
15. Nedić J, Vassilicos JC. Vortex shedding and aerodynamic performance of an airfoil with multi-scale trailing edge modifications. *AIAA J.* 2015;53:1–24.
16. Nedić J, Ganapathisubramani B, Vassilicos JC, Borée J, Brizzi LE, Spohn A. Aeroacoustic Performance of Fractal Spoilers. *AIAA J.* 2012;50:2695–2710.
17. Nedić J, Supponen O, Ganapathisubramani B, Vassilicos JC. Geometrical influence on vortex shedding in turbulent axisymmetric wakes. *Phys Fluids.* 2015;27:1–17.
18. Laizet S, Vassilicos JC. Stirring and scalar transfer by grid-generated turbulence in the presence of a mean scalar gradient. *J Fluid Mech.* 2015;764:52–75.
19. Laizet S, Vassilicos JC. DNS of Fractal-Generated Turbulence. *Flow Turbul Combust.* 2011;87:673–705.
20. Goh KHH, Geipel P, Lindstedt RP. Lean premixed opposed jet flames in fractal grid generated multiscale turbulence. *Combust Flame.* 2014;161:2419–2434.
21. Lane GL, Rigby GD, Evans GM. Pressure Distribution on the Surface of Rushton Turbine Blades - Experimental Measurement and Prediction by CFD. *J Chem Eng Jpn.* 2001;34:613–620.
22. Furukawa H, Kato Y, Inoue Y, Kato T, Tada Y, Hashimoto S. Correlation of Power Consumption for Several Kinds of Mixing Impellers. *Int J Chem Eng.* 2012;2012.
23. Tay M, Tatterson GB. Form and Skin Drag Contributions to Power Consumption for the Pitched-Blade Turbine. *AIChE J.* 1985;31:1915–1918.
24. Mochizuki M, Takashima I. Distribution of Pressure and Velocity on the Surface of Agitator Blade. *Kagaku Kogaku Ronbun.* 1974;38:249–254.

25. Mochizuki M, Sato H, Doida Y, Saita Y, Amanuma T, Takahashi T. Pressure Distribution on the Blade Surface and Form Drag of Impeller in Gas-Liquid Stirred Vessel with a Disk Turbine. *Kagaku Kogaku Ronbun.* 2008;34:557–561.
26. Paul EL, Atiemo-Obeng VA, Kresta SM. *Handbook of Industrial Mixing: Science and Practice.* New York: John Wiley & Sons, Inc., 2004.
27. Scargiali F, Busciglio A, Grisa F, et al. Power Consumption in Uncovered Unbaffled Stirred Tanks: Influence of the Viscosity and Flow Regime. *Ind Eng Chem Res.* 2013;52:14998–15005.
28. Busciglio A, Grisafi F, Scargiali F, Brucato A. Mixing dynamics in uncovered unbaffled stirred tanks. *Chem Eng J.* 2014;254:210–219.
29. Anandha Rao M, Brodkey RS. Continuous flow stirred tank turbulence parameters in the impeller stream. *Chem Eng Sci.* 1972;27:137–156.
30. Xanthopoulos C, Stamatoudis M. Turbulent Range Impeller Power Numbers in Closed Cylindrical and Square Vessels. *Chem Eng Commun.* 1986;46:123–128.
31. King RL, Hiller RA, Tatterson GB. Power consumption in a mixer. *AIChE J.* 1988;34:506–509.
32. Kresta SM, Mao D, Roussinova V. Batch blend time in square stirred tanks. *Chem Eng Sci.* 2006;61:2823–2825.
33. Van't Riet K, Smith JM. The trailing vortex system produced by Rushton turbine agitators. *Chem Eng Sci.* 1975;30:1093–1105.
34. Nagata S. *Mixing: Principles and Applications.* New York: John Wiley & Sons, Inc., 1975.
35. Maynes D, Butcher M. Steady-State and Decay Dynamics for Impellers of Varying Aspect Ratio in Unbaffled Tanks. *AIChE J.* 2002;48:38–49.
36. Bates LR, Fondy PL, Corpstein RR. An examination of some geometric parameters of impeller power. *Ind Eng Chem Process Des Dev.* 1963;2:310–314.
37. Yoon HS, Hill DF, Balachandar S, Adrian RJ, Ha MY. Reynolds number scaling of flow in a Rushton turbine stirred tank. Part I - Mean flow, circular jet and tip vortex scaling. *Chem Eng Sci.* 2005;60:3169–3183.
38. Gunkel AA, Weber ME. Flow Phenomena in Stirred Tanks: I. The Impeller Stream. *AIChE J.* 1975;21:931–939.
39. Unadkat H, Rielly CD, Nagy ZK. PIV study of the flow field generated by a sawtooth impeller. *Chem Eng Sci.* 2011;66:5374–5387.

## Appendix A. $C_D$ and CoP accuracy assessment for the fractal blade

It is important to discuss how the overestimation in torque, attributed to a lack of resolution in the fractal case in section "Pressure integration versus shaft torque", could influence the conclusions drawn regarding the differences in $C_D$ and CoP for the fractal and regular blades. In the case of $C_D$, a possible overestimation for the fractal turbine can only make the difference between the two blades larger, and therefore doesn't affect the conclusions. Regarding the centres of pressure however, it is necessary to assess whether an increased resolution could lead to a consistent difference with the fractal blade, as measured in section "Drag coefficients and centres of pressure".

A way to test that, is to consider a variety of possible $C_p$ distributions on the areas with low measurement resolution, where the boundary effects could be significant (grey areas on blade in fig A.15), and then test whether the CoPs are sensitive to these distributions or not.

Three possible distributions were tested (fig A.14), a parabolic (F1Par), a triangular (F1Tr), and the extreme case where the $C_p$ was assumed zero in the control areas (F1Zero). In the parabolic and the triangular distributions the centreline was assigned the measured value, and then the $C_p$ values dropped parabolically and linearly respectively, until zero in the edges of the area. Torque and CoPs were calculated by multiplying the $C_p$ values of the areas, by a "correction factor" $c_f$: $c_f = 1$ if the $C_p$ distribution is assumed constant, $c_f = 2/3$ for parabolic distribution, $c_f = 1/2$ for triangular distribution and $c_f = 0$ for zero $C_p$ distribution.

In table A.3 listed are the calculated CoPs for the fractal blade using the different distributions, along with the CoPs for the regular blade. The CoPs of the fractal blade are consistently larger than those of the regular blade for the parabolic and triangular distributions, while even in the extreme case of zero $C_p$ distribution the CoP values are approximately the same as the regular blade. The above suggest that the centres of pressure positions of the fractal blade are not severely influenced by the lack of resolution, maintaining consistently higher values compared to the regular blade. The conclusions drawn in paragraph "Drag coefficients and centres of pressure" are therefore not affected by the lack of resolution.

In fig A.15, plotted are the measured shaft torque values, the torques calculated from pressure integration, and the torques from pressure integration, using the parabolic distribution correction, for the fractal1 impeller. From the graph it is obvious that torque calculated though pressure integration is somewhat overestimated. However, after the parabolic correction, the pressure integrated torque agrees well with the shaft torque measurements, showing that boundary effects may indeed cause substantial error when calculating torque from blade pressure measurements.

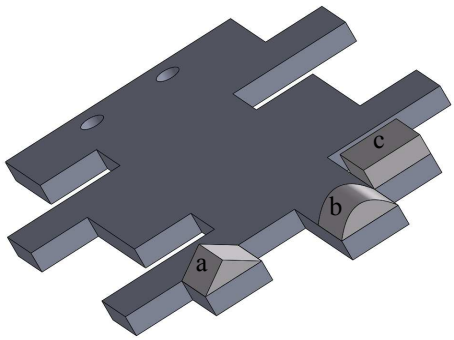


Figure A.14: Different $C_p$ distributions. a) triangular, b) parabolic, c) constant.

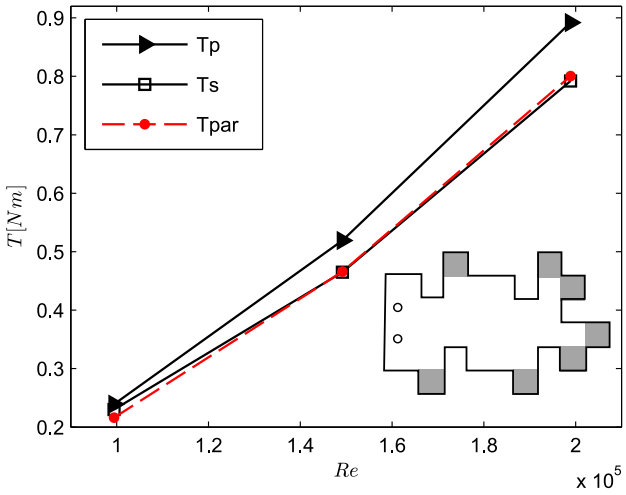


Figure A.15: Variation of the torque of the fractal1 impeller with *Re*. Tp: torque calculated from pressure integration. Ts: torque measured from the shaft. Tpar: torque calculated from pressure integration, using the parabolic correction on the grey areas of the depicted fractal blade.

| Re | Reg | F1 | F1Par | F1Tr | F1Zero |
|---|---|---|---|---|---|
| 100,000 | 91.4 | 94.1 | 93.4 | 93.1 | 91.7 |
| 150,000 | 92.4 | 94.8 | 94.1 | 93.8 | 92.3 |
| 200,000 | 92.7 | 95.1 | 94.6 | 94.2 | 92.9 |

Table A.3: Centres of pressure radii of the regular blade, and the fractal blade with one iteration, using different correction distributions.